SAND RIPPLE CHARACTERIZATION USING AN EXTENDED SYNTHETIC APERTURE SONAR MODEL AND MCMC SAMPLING METHODS

*Alina Zare**, *James T. Cobb*†

*Electrical and Computer Engineering, University of Missouri, Columbia, MO 65211
†Naval Surface Warfare Center, Panama City, FL 32407

ABSTRACT

Side-look synthetic aperture sonar (SAS) can produce very high quality images of the sea-floor. The aim of this work is to develop a hierarchical Bayesian framework for estimating sand ripple characteristics from SAS imagery that can make use of multiple passes over an area at a variety of ranges. Using a hierarchical Bayesian framework and given a known sensing geometry, a method for estimating bathymetry and sand ripple frequency values from single SAS images as well as sets of SAS imagery over an area is presented. This is accomplished through the development of an extended model for sand ripple characterization and a Metropolis-Hastings sampler to estimate bathymetry and sand ripple frequency characteristics for multi-aspect high-frequency side-look sonar data. This hierarchical Bayesian framework allows prior information obtained from previous passes over an area to aid in refining bathymetry and frequency estimates through the use of prior distributions on these values. Results are presented on synthetic and real SAS imagery that indicate the ability of the proposed method to estimate desired sand ripple characteristics.

1. INTRODUCTION

High-resolution imaging sonars, such as side-look synthetic aperture sonar (SAS), can produce near photographic-quality images of the seafloor. Natural textures such as sand ripples formed by current-sediment interaction are easily identifiable to human eye in these images. In this paper, we seek to estimate the salient features of these sand ripple beds using a model that encompasses the sensing geometry of a side-look SAS system and the backscattered return from the rippled seafloor. The model yields parameters, such as frequency and amplitude, that are invariant to sensor range and altitude so that multiple views or passes over the same region can be included in an estimation algorithm.

A stochastic model for Synthetic Aperture Sonar (SAS) imagery collected over sand ripple, originally proposed by Lyons, et al. [6], represents the image as a product between a process governing the speckle in the imagery, $Z(r,x)$, and a process governing the amplitude of a pixel's scattering strength, $a(r,x)$,

$$Y(r,x) = Z(r,x)a(r,x) \tag{1}$$

where r and x are the down-range and cross-range image dimensions, respectively. In this model, considering only the down-range dimension, r, the amplitude of a pixel's scattering strength is approximated by

$$a(r) \simeq \sigma_s(\theta_0) + \left[\sigma_s\left(\theta_{max}\right) - \sigma_s\left(\theta_{min}\right)\right] \frac{g(r) - \bar{g}}{g_{max} - g_{min}}, \tag{2}$$

where $\sigma_s(\theta)$ is the scattering cross section at the grazing angle θ and $g(r)$ is the slope of seafloor at range r. The max and min values are the extremal values of θ and g around the local grazing angle, and $\bar{g}$ is the average slope. Equation 2 is graphically depicted in Figure 1. When computing $\sigma_s\left(\theta\right)$ using a Normal distribution function centered at $\theta = \frac{\pi}{2}$ and using a sine wave as the bathymetry profile, a synthetic ripple field can be generated using this model. An example of a synthetic ripple field generated using this model is shown in Figure 2.

In this work, this original model is expanded to define a scattering cross-section function that incorporates the occlusion from preceding peaks in the sand ripple field. Then, using this expanded model, the parameters governing the bathymetry profile (i.e. the frequency and the amplitude of the peaks in the sand ripple height field) are estimated from SAS imagery using a hierarchical Bayesian framework in conjunction with a Metropolis-Hastings sampling algorithm. The proposed hierarchical Bayesian framework allows previous estimates of the bathymetry and sand ripple frequency characteristics from previous aspects and passes over an area to guide refinements of these parameters through the use of prior distribution functions.

Accurate estimates of the bathymetry and sand ripple frequency characteristics can be ultimately used during a number of applications of SAS imagery including detection and classification of targets in a scene [3, 4], seabed segmentation and classification [1, 2], and others. Previous work in sand ripple characterization include measuring wave-formed sand ripples using an acoustic multiple transducer array [5] and analyzing side-scan sonar data using fingerprint analysis techniques [8].

978-0-933957-40-4 ©2013 MTS

In the following, the expanded sand ripple field model is defined in Section 2. Section 3 describes the proposed hierarchical Bayesian framework and the Metropolis-Hastings sampling algorithm used to estimate the desired parameters from both single passes over an area and using multiple aspects and passes over an area at a variety of ranges. Section 4 includes experimental results on simulated and real SAS imagery. Section 5 includes a summary and discussion on future work.

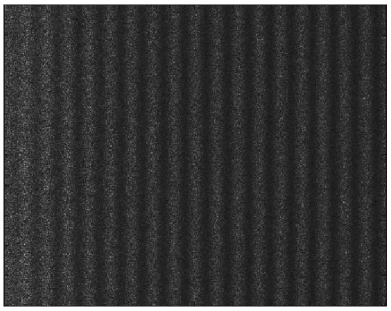

Fig. 2. Synthetic ripple field generated using the model in [6] with a sine wave bathymetry profile. The speckle term, $Z(x, y)$ for this image was generated using a Rayleigh distributed speckle with a parameter value of $\alpha = 1 \times 10^2$.

2. EXPANDED SAND RIPPLE MODEL

The original model, shown in (2), is expanded to include a scattering cross-section function that incorporates occlusion or scattering from the trough ripple by the preceding peaks. In this expanded model a function ψ_s replaces σ_s in (2),

$$a^*(r, A_H, f) \simeq \tag{3}$$
$$\psi_s(\theta_0, r) + [\psi_s(\theta_{max}, r) - \psi_s(\theta_{min}, r)] \frac{g(r) - \bar{g}}{g_{max} - g_{min}},$$

where

$$\psi_s(\theta, r) \triangleq \begin{cases} 0 & \text{if } A_H - \frac{A_S \cdot g(r)}{r - g(r)} \geq h(r) \\ \sigma_s(\theta) & otherwise \end{cases}, \tag{4}$$

A_H is the amplitude or maximum ripple height, A_S is the height of the SAS array from the sea floor, and $h(r)$ is the ripple height at range r. Note that an estimate of A_S is measured and provided by the SAS sensor for each downrange location. However, the A_S value is dependent on the sea-floor characteristics below the sensor. For example, if the SAS array is located above sand ripple, then the A_S value will depend on whether the measurement is collected over a peak or trough of the sand ripple.

Given a bathymetry profile approximated by a sine curve, the ripple height at range r is defined as $h(r) \simeq A_H \sin(2\pi f r + b)$ where f and b are the sand ripple frequency and phase values, respectively. The ripple slope field at range r, can then be computed as $h'(r) = g(r) \simeq 2\pi f A_H \cos(2\pi f r)$. A graphic illustration of the role the additional variables play is depicted in Figure 3 and a synthetic ripple field generated from this model is shown in Figure 4. The trough of the synthetic ripple in Figure 4 is clearly occluded at longer ranges. Therefore, this expanded model extends the original model to approximate SAS pixel scattering strength for a larger set of range values by accounting for these shadowed or occluded regions.

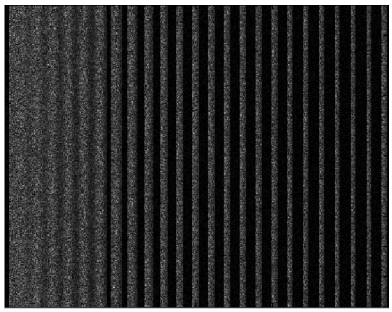

Fig. 4. Synthetic ripple field displaying occluded pixels in the trough at long ranges. These shadowed or occluded pixels are typically seen in real imagery. The speckle term, $Z(x, y)$ for this image was generated using a Rayleigh distributed speckle with a parameter value of $\alpha = 1 \times 10^2$.

3. HIERARCHICAL BAYESIAN FRAMEWORK AND METROPOLIS-HASTINGS SAMPLER

The proposed method estimates the sand ripple bathymetry by estimating the maximum ripple height, A_H and the frequency of the sand ripple field, f, using a Metropolis-Hastings sampling algorithm [7]. This approach was taken since the Metropolis-Hastings sampler provides the advantage of being able to estimate parameter values given complex data likelihood and prior distribution while maintaining the convergence guarantees to a global optimum of an MCMC sampling approach.

3.1. Hierarchical Bayesian Framework

The likelihood used in the proposed framework places a Gaussian distribution around an input SAS pixel value given its estimate with the expanded model of the amplitude of the pixel's scattering strength,

$$x_{i,r} | A_H, f \sim N\left(x_{i,r} | a^*(r, A_H, f), 1\right), \tag{5}$$

where $x_{i,r}$ is the i^{th} pixel in the image at range r. Then, the likelihood over a SAS image can be defined as shown in (6),

$$\mathbf{X} | A_H, f \sim \prod_{i=1}^{N} N\left(x_{i,r} | a^*(r, A_H, f), 1\right), \tag{6}$$

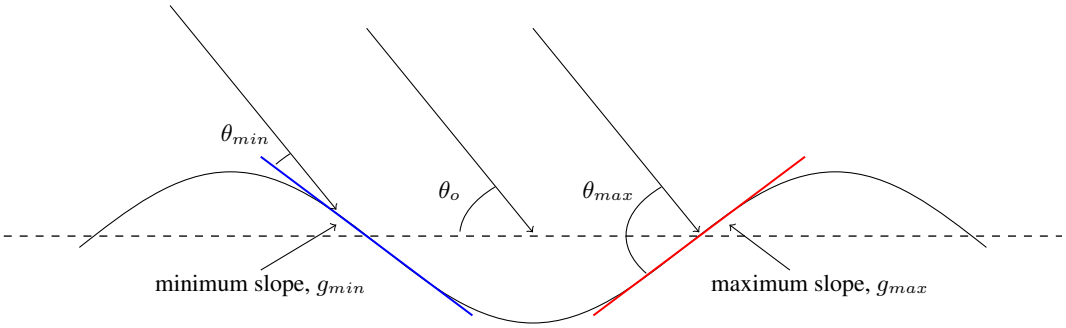

Fig. 1. Graphic depiction of the original sand ripple scattering model from [6]

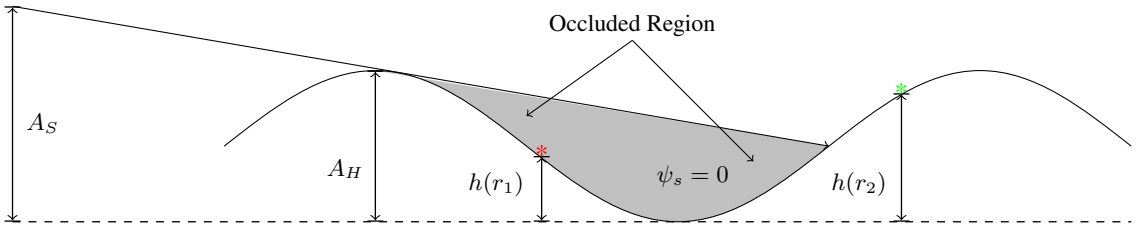

Fig. 3. The expanded model that accounts for shallow grazing angles at long ranges by including the case of occlusion in the trough of the ripple. The red asterisk is obscured by the preceding peak, while the green asterisk is visible by the sonar.

where N is the total number of pixels in the SAS image under consideration and X is the set of all image pixels. By sampling the A_H and f values that maximize the likelihood function in (6), the mean squared error between the estimate given the model in (4) and the estimated sand ripple characteristics and the input data, $\mathbf{X}$, is minimized.

In order to constrain the sand ripple characteristics to physically possible values and incorporate any prior information, Truncated Gaussian prior distributions are placed on the A_H and f values,

$$A_H \sim N_t(A_H|\mu_{A_H}, \sigma_{A_H}, l_{A_H}, u_{A_H}) \tag{7}$$

and

$$f \sim N_t(A_H|\mu_f, \sigma_f, l_f, u_f) \tag{8}$$

where

$$N_t(x|\mu, \sigma, l, u) = \begin{cases} CN\,(x|\mu, \sigma) & \text{if } l \leq x \leq u \\ 0 & otherwise \end{cases}, \tag{9}$$

where C is the normalization constant for a truncated Gaussian distribution. The lower and upper truncation points, l_{A_H}, u_{A_H}, l_f, and, u_f are set to constrain the maximum ripple height and frequency to physically possible values. These values may also be assigned given additional oceanographic information such as sediment type, etc. The prior parameter values $(\mu_{A_H}, \sigma_{A_H}, \mu_f, \sigma_f)$ are set based on estimates given previous passes over the sand ripple field under consideration as described in subsequent sections.

3.2. Sampling Method

The proposed method iteratively samples A_H and f using a Metropolis-Hastings algorithm [7]. The sampling algorithm for estimating the values given a single pass of the data is summarized in the psuedo-code in Algorithm 1. In the following, each step of the sampling algorithm and initialization is described.

3.2.1. Sample Frequency

As in a standard Metropolis-Hastings algorithm, a proposal distribution is used to generate samples of the parameters of interest for evaluation in the posterior distribution (proportional to the assumed data likelihood and prior distributions) to be maximized. In the current implementation, the proposal distribution used to sample a new sand ripple frequency estimate, f^{new}, is a Gaussian mixture centered on the previous frequency sample value, f^{old},

$$p(f^{new}|f^{old}) = \\ w_{n,f}N(f^{new}|f^{old}, \quad s_{n,f}) + w_{w,f}N(f^{new}|f^{old}, s_{w,f}) \tag{10}$$

where $w_{n,f}$ and $w_{w,f}$ are a fixed parameters such that $w_{w,f} + w_{n,f} = 1$ and $w_{n,f}, w_{w,f} \geq 0$. These are used to determine the relative frequency sampling from a Gaussian whose variance is either relatively small (narrow spread: $s_{n,f}$) or large (wide spread: $s_{w,f}$). The variance values, $s_{n,f}$ and $s_{w,f}$, are fixed values used to generate the frequency samples. When sampling from the narrow Gaussian mixture component, a

Algorithm 1 - SAS Bathymetry Sampling Method: *A Metropolis-Hastings sampler that estimates sand ripple field height and frequency. The method used for each step is described in the section shown in parentheses*

1: Set parameter values and initialize A_H and f (Section 3.2.3)
2: **for** $k \leftarrow 1$ to number of total iterations **do**
3: Sample the ripple field frequency, f (Section 3.2.1)
4: Sample the ripple field height, A_H (Section 3.2.2)
5: **end for**

small area in the parameter space surrounding the current frequency sample is explored to refine the current frequency estimate. Sampling from the proposal distribution using the wide Gaussian mixture component allows for more large exploration of the parameter space. Therefore, the $w_{n,f}, w_{w,f}, s_{n,f}$ and $s_{w,f}$ values will affect the speed of convergence of the proposed method by balancing the local versus global search parameters. Given this proposal distribution, the acceptance ratio for the frequency values used to evaluate f^{new} will be

$$\begin{aligned} a &= \frac{\Pi(f^{new}|\mathbf{X}, A_H)}{p(f^{new}|f^{old})} \frac{p(f^{old}|f^{new})}{\Pi(f^{old}|\mathbf{X}, A_H)} \\ &= \frac{\Pi(f^{new}|\mathbf{X}, A_H)}{\Pi(f^{old}|\mathbf{X}, A_H)} \end{aligned} \quad (11)$$

where

$$\Pi(f|\mathbf{X}, A_H) \propto \quad (12)$$
$$\prod_{i=1}^{N} N\left(x_{i,r}|a^*(r, A_H, f), 1\right) N_t(f|\mu_f, \sigma_f, l_f, u_f)$$

with $N_t(f|\mu_f, \sigma_f, l_f, u_f)$ as the truncated Gaussian prior distribution in (8) and the second equality is the result of the proposal distribution being a symmetric distribution.

3.2.2. Sample Ripple Field Height

The sampling step for the ripple field height parallels the step used for sampling the frequency. Again, the proposal distribution is a Gaussian mixture centered on the previous A_H value,

$$\begin{aligned} &p(A_H^{new}|A_H^{old}) = w_{n,A} N(A_H^{new}|A_H^{old}, s_{n,A}) \quad (13) \\ &+(1 - w_{n,A}) N(A_H^{new}|A_H^{old}, s_{w,A}). \end{aligned}$$

Given that the proposal distribution is symmetric, the acceptance ratio used is

$$a = \frac{\Pi(A_H^{new}|\mathbf{X}, f)}{\Pi(A_H^{old}|\mathbf{X}, f)} \quad (14)$$

where

$$\Pi(A_H|\mathbf{X}, f) \propto \quad (15)$$
$$\prod_{i=1}^{N} N\left(x_{i,r}|a^*(r, A_H, f), 1\right) N_t(A_H|\mu_{A_H}, \sigma_{A_H}, l_{A_H}, u_{A_H}).$$

3.2.3. Initialization and Parameter Settings

The proposed sampling method requires several parameters to be set prior to running the algorithm. For our current implementation and all experimental results shown, initialization for the algorithm and parameters are determined using the following methods.

Initialization: Initial values for the frequency are determined by first averaging the SAS image clip being considered cross-range and, then, using the averaged signal to estimate the frequency using a 1-D FFT. The SAS image clip being considered contains the input pixels $\mathbf{X}$. In the experiments shown here, the image clip considered in both the simulated and real SAS imagery are generally 500×500 pixels in size. The A_H values are initialized to the root mean square of the SAS image clip.

Prior to sampling, the SAS image clip being analyzed is smoothed and normalized. Smoothing is done by applying a 2-D median filter to the image clip and is done to minimize the speckle term in (1) (since the pixel scattering strength, $a(r)$, is the term of interest). After smoothing, the image is normalized by subtracting the mean image pixel value and dividing by the maximum image pixel value.

Parameter Settings: In the current implementation, the phase value, b, is fixed to zero. The amplitude of the SAS array, A_S is assumed to be known as well as the approximate range value, r, for each pixel in the image clip.

The scattering cross section, $\sigma_S(\theta)$ used in the $\psi_S(\theta, r)$ function is modeled using a Gaussian distribution centered at a grazing angle of $\frac{\pi}{2}$ since a grazing angle perpendicular to the ripple height field is expected to provide the largest return. In our implementation, the variance of the Gaussian used to model the scattering cross section is set to $\frac{\pi}{3}$. This variance value was set based on comparisons between data simulated using this model and collected SAS imagery.

When sampling the field height and frequency, the parameters of their corresponding truncated prior Gaussian distributions need to be set. The upper and lower truncation points are set to constrain the frequency and height parameters to physically possible value. In our current implementation, these upper and lower truncation points are set to 0 and 1 for both f and A_H. However, these values can be easily modified given further constraining prior information (such as prior constrained information derived from oceanographic data).

Parameters for the proposal distributions for f and A_H in-

clude $w_{n,f}$, $w_{n,A}$, $s_{n,f}$, $s_{n,A}$, $s_{w,f}$, and $s_{w,A}$. In the current implementation, these values are set to 0.7, 0.7, 0.01, 0.01, 0.1, and 0.1, respectively. Given that the proposed method is a Metropolis-Hastings algorithm, it will benefit from the corresponding convergence guarantees. However, the speed of convergence is dependent on these parameter settings. Future work can include investigating methods to optimizing these proposal distribution parameters.

When given only an initial single pass of the data, uninformative priors are used for both of these parameters of interest (as opposed to the truncated Gaussian distributions defined in the previous section). These uninformative priors can be approximated by setting the σ_f and σ_{A_H} value to extremely large variance values relative to the truncation points of the prior. However, when previous aspects and passes over an area of interest have been analyzed, the frequency and ripple field height estimates obtained from the previous passes can be used to set the prior distribution parameter settings. In these cases, μ_f and μ_{A_H} can be set to the values estimated from previous passes and, σ_f and σ_{A_H} can be set based on the confidence of these previous estimates. In our implementation, σ_f and σ_{A_H} are set based of the average error found when estimating these values from a single pass on simulated data set (in which the true f and A_H values are known).

4. EXPERIMENTAL RESULTS

The proposed sampling method was applied to simulated and real SAS imagery. Results are shown on these data sets and discussed in the following sections.

4.1. Simulated SAS Data - One Pass

The proposed method was run on simulated data generated using the model defined in (1) with the expanded pixel scattering strength model shown in (3). The speckle term, $Z(x, y)$ in (1) was generated using a Rayleigh distributed speckle with a parameter value of $\alpha = 1 \times 10^2$. An example of the simulated imagery is shown in Figure 4.

This initial experiment was run using only single images (i.e. one pass over an area). Therefore, uninformative prior distributions over the physically possible constrained range were used and approximated using large variance values in the priors described in (7) and (8).

This single pass experiment was repeated three times so that the true f, A_H, and range values were varied in one of these experiments and held constant during the other two.

4.1.1. Varying the true f value

In this experiment, the f values were varied to be 0.4, 0.5, 0.6 and 0.7 while the A_H value was set to 0.07m and the image clip ranged from 24.4m to 36.6m in range. In all simulated experiments the height of the SAS array was fixed to 4.83m. For each f value, the algorithm was run 10 times and a new simulated image was generated for each run. In the following tables, the mean squared error ($\pm$ one standard deviation) is shown for both the estimated f and A_H values over the 10 runs. Results are shown in Table 1. As shown in the Table 1, even with only one SAS image, the f value was consistently accurately estimated with squared errors on the order of 1×10^{-4}.

4.1.2. Varying the true A_H value

The A_H values were varied to be 0.06m, 0.07m, 0.08m and 0.09m while the f value was set to 0.6 and the image clip ranged from 24.4m to 36.6m in range. Again, for each A_H value, the algorithm was run 10 times and a new simulated image was generated for each run. Results are shown in Table 2. As shown in Table 2, more accurate results are obtained with larger A_H values. This occurs because at larger amplitudes, more shadowed and occluded areas are seen in the imagery. The shadowed/occluded regions provide more information about the scene and are leveraged by the expanded SAS sand ripple model to provide better estimates of bathymetry and sand ripple characteristics.

4.1.3. Varying the range of the simulated SAS imagery

The range values were varied from 1.2m to 13.4m in range to 36.6m to 48.2m in range while the A_H value was set to 0.07m and the f value was fixed to 0.6. For each range, the algorithm was run 10 times and a new simulated image was generated for each run. Results are shown in Table 3. As shown in Table 3, the accuracy of the A_H estimates are very dependent on the distance from the SAS array to the imaged area. Accuracy increases in the larger range values because at longer ranges additional information is garnered from the shadowed/occluded image pixels. At close range, shadowed and occluded regions do not occur to aid in estimating the bathymetry. By defining the expanded sand ripple model, bathymetry estimates can be drawn from a single SAS image using the occluded regions.

4.2. Simulated SAS Data - Multiple Passes

In this experiment, multiple passes over an area with different sensing geometries are used to iteratively apply the proposed method and refine the sand ripple frequency and amplitude parameter estimates. Considering the results from the first experiment, it can be seen that, using only one pass of the data, the sand ripple frequency estimates have much higher accuracy rates. Given these results, when conducting multi-aspect experiments, the prior distribution for the frequency is set to a much stronger prior (i.e. a lower variance σ_f) than the A_H prior distribution. In practice, the σ_f and σ_{A_H} values were set based on the squared error computed from simulated data experiments with corresponding parameter settings.

True f Value	0.4	0.5	0.6	0.7
A_H	0.806 ($\pm$ 0.04)m	0.303 ($\pm$ 0.13)m	0.002 ($\pm$ 0.001)m	0.002 ($\pm$ 0.002)m
f	3×10^{-5} ($\pm$ 6×10^{-6})	3×10^{-5} ($\pm$ 3×10^{-6})	1×10^{-6} ($\pm$ 3×10^{-6})	1×10^{-6} ($\pm$ 5×10^{-6})

Table 1. One Pass Simulated Data: Varying f, Average Squared Error ($\pm$ 1 standard deviation)

True A_H	0.06m	0.07m	0.08m	0.09m
A_H	0.13 ($\pm$ 0.15)m	0.002 ($\pm$ 0.002)m	0.002 ($\pm$ 0.001)m	0.004 ($\pm$ 0.002)m
f	1×10^{-5} ($\pm$ 7×10^{-6})	1×10^{-5} ($\pm$ 3×10^{-6})	1×10^{-5} ($\pm$ 3×10^{-6})	1×10^{-5} ($\pm$ 2×10^{-6})

Table 2. One Pass Simulated Data: Varying A_H, Average Squared Error ($\pm$ 1 standard deviation)

To evaluate the proposed method with a multi-aspect experiment, simulated data was generated for the same area from two different range values (12.2-24.4m and 24.4-36.6m). An example of data simulating two-passes over the same area at different range values is shown in Figure 5. The true f and A_H values were fixed to 0.6 and 0.07m, respectively, for all runs of the experiment. First, the proposed sampling algorithm was applied to the simulated initial pass of the data with a collection range of 12.2-24.4m. Then, using these initial estimates, and the average squared error for these parameters from a single pass extracted from Experiment 1, the prior distribution parameter settings were set to $\sigma_f = 0.003$ and $\sigma_{A_H} = 0.17$ with mean values μ_f and μ_{A_H} set to the frequency and amplitude estimated from the first pass of the data. Given these prior parameter settings, the simulated second pass of the area was analyzed with the proposed sampling algorithm. The resulting f and A_H parameter estimates for five runs of this experiment are shown in Table 4. As shown in Table 4, the accuracy of the frequency and amplitude increase given the second pass over the area of interest.

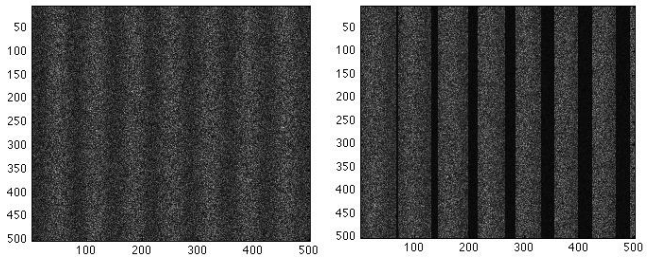

(a) Synthetic Ripple Field - Pass 1 (b) Synthetic Ripple Field - Pass 2

Fig. 5. Synthetic ripple imagery over the same area with two different aspect ranges (a) 12.2-24.4m in range and (b) 24.4-36.6m in range. The speckle term, $Z(x, y)$ for this image was generated using a Rayleigh distributed speckle with a parameter value of $\alpha = 1 \times 10^2$.

4.3. SAS Data

Finally, the proposed sampling algorithm was applied to a single pass of real SAS imagery. The SAS image clip used is shown in Figure 6 (a). The resulting estimated f and A_H parameters were 0.69 and 0.2m, respectively. A simulated SAS image generated from the expanded model using these estimated parameters is shown in Figure 6 (b).

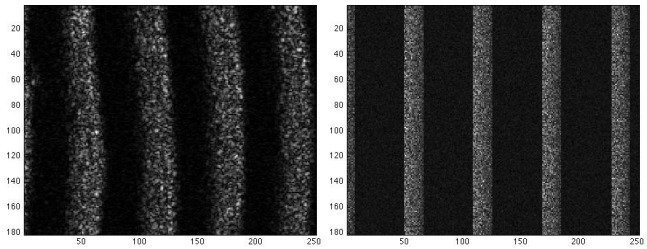

(a) Real SAS Imagery (b) Synthetic Ripple Field

Fig. 6. (a) SAS imagery collected with an average sonar array height of 5.05 at ranges values from 30.5 to 36.6m. (b) Synthetic ripple imagery generated using the parameter estimates found by the sampling algorithm on the SAS imagery shown in (a).

5. FUTURE WORK

In this paper, an expanded model for sand ripple characterization in SAS imagery is presented. Furthermore, a Metropolis-Hastings sampling approach for estimating the bathymetry and sand ripple frequency characteristics was developed. Future work on this topic includes a number of possibilities such as expanding the sampling method to account for estimating the phase angle, b, in the model. Often, in collected SAS imagery, sand ripples merge and split resulting in different areas of the imagery to be better modeled with different phase values. Future work may also include automating the prior distribution parameter settings, specifically the variance values, for multi-aspect analysis using pixel-wise error values in the initial and previous passes. Currently, this variance is set

Range Values	1.2m - 13.4m	12.2m - 24.4m	24.4m - 36.6m	36.6m - 48.2m
A_H	0.24 ($\pm$ 0.18)m	0.62 ($\pm$ 0.12)m	0.001 ($\pm 1 \times 10^{-3}$)m	0.002 ($\pm 8 \times 10^{-4}$)m
f	0.34 ($\pm 2 \times 10^{-4}$)	8×10^{-5} ($\pm\ 2 \times 10^{-5}$)	1×10^{-5} ($\pm\ 8 \times 10^{-6}$)	6×10^{-6} ($\pm\ 4 \times 10^{-6}$)

Table 3. One Pass Simulated Data: Varying Range, Average Squared Error ($\pm$ 1 standard deviation)

	Pass 1		Pass 2	
Experiment	A_H Squared Error	f Squared Error	A_H Squared Error	f Squared Error
1	0.7	0.07×10^{-3}	0.003	0.01×10^{-3}
2	0.6	0.07×10^{-3}	0.061	0.01×10^{-3}
3	0.8	0.07×10^{-3}	0.033	0.01×10^{-3}
4	0.7	0.11×10^{-3}	0.005	0.07×10^{-3}
5	0.6	0.07×10^{-3}	0.016	0.07×10^{-3}

Table 4. One Pass Simulated Data: Varying Range, Average Squared Error ($\pm$ 1 standard deviation)

based on independent single-pass experiments. However, future work may include setting these parameter values based on information extracted from the previous imagery or additional oceanographic data. Also, the expanded model presented here covers a single aspect angle (i.e. an angle perpendicular to the sand ripple). However, the areas of occlusion and the pixel scattering cross section highly depend on aspect angle. Given this dependence, the accuracy of sand ripple characteristics are dependent on this angle as well. Future work will include incorporating aspect angle into the extended model to provide more flexibility in the proposed approach and, based on aspect angle and range, assign confidence levels to the estimated parameter values. Finally, in the current method, the bathymetry profile was assumed to be a sine curve. However, more appropriate models may include the Stokes function or $\cos^2$ as the bathymetry profile allowing for more peaked sand ripples.

6. REFERENCES

[1] J. Cobb and J. Principe. Autocorrelation features for synthetic aperture sonar image seabed segmentation. In *Systems, Man, and Cybernetics (SMC), 2011 IEEE International Conference on*, pages 3341 –3346, oct. 2011.

[2] J. T. Cobb and J. Principe. Seabed segmentation in synthetic aperture sonar images. In *Proceedings of the SPIE*, pages 80170M–80170M–11, 2011.

[3] G. Dobeck. Algorithm fusion for automated sea mine detection and classification. In *OCEANS, 2001. MTS/IEEE Conference and Exhibition*, volume 1, pages 130 –134 vol.1, 2001.

[4] G. J. Dobeck and J. T. Cobb. Fusion of multiple quadratic penalty function support vector machines (qpfsvm) for automated sea mine detection and classification. In *Proceedings of the SPIE*, pages 401–411, 2002.

[5] D. M. Hanes, V. Alymov, and Y. S. Chang. Wave-formed sand ripples at duck, north carolina. *Journal of Geophysical Research*, 106(C10):22575–22592, Oct 2001.

[6] A. Lyons, D. Abraham, and S. Johnson. Modeling the effect of seafloor ripples on synthetic aperture sonar speckle statistics. *Oceanic Engineering, IEEE Journal of*, 35(2):242 –249, april 2010.

[7] C. S. and G. E. Understanding the metropolis-hastings algorithm. *The American Statistician*, 49(4):327–335, april 1995.

[8] A. Skarke and A. C. Trembanis. Parameterization of bedform morphology and defect density with fingerprint analysis techniques. *Continental Shelf Research*, 31(16):1688 – 1700, 2011.